

Dynamic Heterogeneity In The Monoclinic Phase Of

CCl_4

Nirvana B. Caballero ^{*,†} Mariano Zuriaga ^{*,†} Marcelo Carignano ^{*,‡} and Pablo
Serra ^{*,†}

*Facultad de Matemática, Astronomía y Física, Universidad Nacional de Córdoba, Córdoba,
Argentina and IFEG-CONICET, Ciudad Universitaria, X5016LAE Córdoba, Argentina, and
Qatar Environment and Energy Research Institute, Hamad Bin Khalifa University, Qatar
Foundation, P.O. Box 5825, Doha, Qatar*

E-mail: ncaballe@famaf.unc.edu.ar; zuriaga@famaf.unc.edu.ar; mcarignano@qf.org.qa;
serra@famaf.unc.edu.ar

Phone: +54(0)3514334051, ext. 218. Fax: +54(0)3514334054

*To whom correspondence should be addressed

[†]Facultad de Matemática, Astronomía y Física, Universidad Nacional de Córdoba, Córdoba, Argentina and IFEG-CONICET, Ciudad Universitaria, X5016LAE Córdoba, Argentina

[‡]Qatar Environment and Energy Research Institute, Hamad Bin Khalifa University, Qatar Foundation, P.O. Box 5825, Doha, Qatar

Abstract

Carbon tetrachloride (CCl_4) is one of the simplest compounds having a translationally stable monoclinic phase while exhibiting a rich rotational dynamics below 226 K. Recent nuclear quadrupolar resonance (NQR) experiments revealed that the dynamics of CCl_4 is similar to that of the other members of the isostructural series $\text{CBr}_n\text{Cl}_{4-n}$, suggesting that the universal relaxation features of canonical glasses such as α - and β -relaxation are also present in non-glass formers. Using molecular dynamics (MD) simulations we studied the rotational dynamics in the monoclinic phase of CCl_4 . The molecules undergo C_3 type jump-like rotations around each one of the four C-Cl bonds. The rotational dynamics is very well described with a master equation using as the only input the rotational rates measured from the simulated trajectories. It is found that the heterogeneous dynamics emerges from faster and slower modes associated with different rotational axes, which have fixed orientations relative to the crystal and are distributed among the four non-equivalent molecules of the unit cell.

February 2, 2016

Introduction

The currently accepted scenario for canonical glasses includes different relaxation mechanisms that are universally present in all systems. Experimentally, these different mechanisms are clearly revealed by the dielectric spectra that shows a broad low frequency peak referred to as α -relaxation^{1,2} and a higher frequency peak or shoulder usually called Johari-Goldstein β -relaxation.³⁻¹⁴ The α -relaxation is generally attributed to processes involving the cooperative dynamics of regions of molecules.^{1,2} The microscopical origin of the β relaxation is still a matter of wide debate.⁴⁻¹³ The proposed models explain this peak as a consequence of the nonuniformity of the glassy state involving only local regions in which molecules can diffuse (islands of mobility). An alternative homogeneous explanation attributes the secondary relaxation phenomena to small-angle reorientations of all the molecules.¹⁵⁻¹⁷

Systems having translational crystalline order but rotational degrees of freedom also display a glassy behavior. Since in these cases one type of degree of freedom is completely absent, they represent simplified models on which to test theoretical concepts on glassy dynamics.¹⁸⁻²¹ Compounds of molecules of the type $\text{CBr}_n\text{Cl}_{4-n}$, with $n=0,1,2$, are examples of systems with this characteristics.²²⁻²⁴ They have a series of solid-solid phase transitions attributed to the ability of the molecules to acquire rotational degrees of freedom as the temperature is increased. All these compounds crystallize from the melting to a plastic FCC phase. Further reduction of the temperature leads to a $C2/c$ monoclinic phase.²⁵⁻²⁹ The cases $n=1$ and $n=2$ exhibit a glass transition at 90 K that is clearly visible through calorimetric techniques and its structure shows disorder in the position of the Cl and Br atoms.^{30,31} The case $n=0$ cannot display such a disorder and, in fact, the calorimetric curve does not show a glass transition at low temperatures.³⁰

The dielectric spectra of CBrCl_3 and CBr_2Cl_2 was reported by Zuriaga *et al.*²⁴ in the temperature range 100 – 250 K and 100 – 210 K, respectively. At the lower end of the temperature range the most relevant characteristic is that both spectra display a well-defined shoulder on the high frequencies flank of the α -peak, which is attributed to the β -relaxation. Since CCl_4 has no molecular dipole moment it is not accessible to dielectric experiments but it can be studied using

nuclear quadrupolar resonance. Interestingly, the resolution of the NQR spectra for CCl_4 is well superior to the corresponding spectra for CBr_2Cl_2 and CBrCl_3 and the two techniques complement each other. On the other hand, the NQR experiments are limited to a temperature range between 77 K and 140 K, with the upper end determined by the broadening of the signal. The picture that emerges from the combined analysis is that the three compounds have a very similar dynamic evolution in the monoclinic phase as a function of temperature.^{23,24} The analysis of the isostructural CCl_4 shows that nonequivalent molecules in the unit cell perform reorientational jumps at different time scales due to their different crystalline environments. These results support the conclusion that the dynamic heterogeneity is intimately related to the secondary relaxation observed in these compounds.^{23,24,32}

This work is a direct extension of our previous works involving halogenomethanes.^{23,24,32} In this case we have studied the monoclinic phase of CCl_4 using extensive molecular dynamics simulations on a fully anisotropic cell, and the results were compared with an analytical stochastic model. The advantage of this particular system is that it allows for the determination of rotational correlation times from NQR measurements with sufficient precision to distinguish between the nonequivalent groups of molecules. The same distinction is easily done in the molecular dynamics simulations, which in turn allows for an analysis at the individual nonequivalent groups and correlate the results with the location of the molecules in the lattice. The temperature range affordable by the simulations covers from the FCC phase down to 160 K. Simulations at lower temperatures became impossible as the relaxation times go beyond 10 μs . It is found that, when the spin-lattice relaxation times from the experiments and from the simulations are plotted in the 100 – 220 K temperature range, the two sets of curves correspond to each other very well for the five distinguishable modes suggesting that CCl_4 behaves as a strong glass in the whole temperature range, in spite of the fact that the compound cannot glassify due to its lack of orientational entropy.

Theoretical Methods

Model and computational details

CCl_4 is a tetrahedral molecule having three equivalent C_2 and four equivalent C_3 symmetry axes. Following our previous work,³² we have modeled the CCl_4 molecule as a rigid, non-polarizable tetrahedron with the carbon atom at its center and a chlorine atom at each one of the vertices. The interaction between molecules is represented by a combination of Lennard-Jones and Coulombic terms summarized in Table 1. The cross interaction between atoms of different type is calculated by applying the Lorentz-Berthelot combination rules, i.e., geometrical mean for ϵ and arithmetic mean for σ . A spherical cut-off at 1.5 nm was imposed on all intermolecular interactions. Periodic boundary conditions were imposed in all three Cartesian directions.

Table 1: CCl_4 model parameters and geometry.

	ϵ [kJ/mol]	σ [nm]	q [e]	Bond [nm]	
C	0.22761	0.37739	-0.696	C-Cl	0.1766
Cl	1.09453	0.34667	0.174	Cl-Cl	0.2884

The monoclinic crystal structure of CCl_4 , resolved by Cohen et *al.* at 195 K,³³ corresponds to the $C2/c$ space group. The unit cell, which contains $Z=32$ molecules, has the following lattice parameters: $a=2.0181$ nm, $b=1.1350$ nm, $c=1.9761$ nm and angle $\beta = 111.46^\circ$. Using the experimental crystalline structure as initial coordinates, we constructed a simulation supercell containing 512 molecules, which correspond to 16 monoclinic unit cells. This supercell was prepared by replicating the experimental unit cell twice on the x and z directions and four times in the y direction.

The molecular dynamics simulations, conducted under NPT conditions, have been carried out using the Gromacs v5.0.2 simulation package. Atom-atom distances within each molecule were kept constants with the SHAKE algorithm. The simulations were started with a 10 ns equilibration run with the pressure controlled by a Berendsen barostat and the temperature controlled with the v-rescale thermostat. The Berendsen weak coupling method ensured a smooth approach to equilibrium with no disruptions to the simulation cell. The classical Newton's equations were integrated

using the leap-frog algorithm and the time step of the integration of the equations of motion was set to 1 fs.

The production runs were extended up to 100 ns or 10 μ s depending on the temperature, using in this case a time step of 5 fs. The control of the temperature was made by using a Nosé-Hoover thermostat, with a time constant of 2.0 ps. The pressure was maintained constant by using a fully anisotropic Parrinello-Rahman barostat with a reference pressure of 1 atm. The study covered temperatures ranging from 160 K to 230 K, in steps of 10 K. The monoclinic structure was stable in the whole analyzed temperature range (see Supporting Information file).

Results and Discussion

The spatial positions of the molecules in the unit cell of the system are defined through the application of 8 symmetry operations over the 4 nonequivalent molecules (16 Cl atoms with nonequivalent positions). As a consequence, the system has four distinctive groups of molecules that we will refer to as G_I , G_{II} , G_{III} and G_{IV} . In our simulation cell, each group contains 128 molecules. Each molecule belonging to a given group has the same specific arrangement of neighboring molecules. All the molecular reorientation processes occurring during the simulations are sudden large-angle jumps of the Cl atoms. The jumps were detected using a running test algorithm based on a signal to noise measure and adapted from the work of Carter and Cross.³⁴ In this method, the molecular jumps are detected by a spike in the test function as explained in the Supporting Information file. After analyzing the trajectories for all the temperatures, the time t_i of every single jump was registered. The angle described by a C-Cl bond upon a jump was calculated using the average direction of the bond before and after the jump. Namely, defining \vec{b}_j as the bond between the central C atom and the j -th Cl atom of the same molecule, the angle jump at time t_i is defined as the angle between $\langle \vec{b}_j \rangle_{i-1}$ and $\langle \vec{b}_j \rangle_i$. Here, the angular brackets represent time average and the subscript i indicates the lapse between t_i and t_{i+1} . In Figure S1 we show the relative frequency of the reorientation angles calculated from the simulation at 160 K and for the four different groups of molecules. All

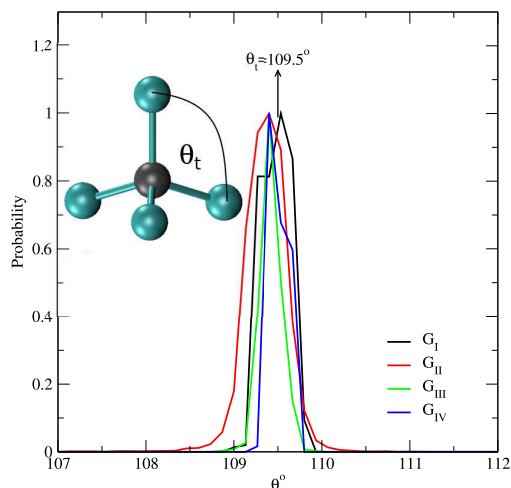


Figure S1: Normalized frequency distribution of reorientation angles for the four distinct group of molecules, as indicated. The results correspond to the production run at 160 K. The maximum at the tetrahedral angle indicate that all jumps are $C3$ type rotations.

the curves peak at the tetrahedral angle, which is the angle that should be observed upon $C3$ type rotations. Indeed, a careful inspection confirmed that for all temperatures there were just a handful of cases corresponding to $C2$ type rotations and therefore there were neglected in the analysis.

In order to characterize the molecular rotations using standard self correlation methods, we calculate the relaxation of the bond orientation through self correlation functions defined as

$$C_j(t) = \langle \vec{b}_j(0) \cdot \vec{b}_j(t) \rangle, \quad (1)$$

where $j = 1, \dots, 4$ represents a particular C-Cl bond, $\vec{b}_j(0)$ represents the position of the C-Cl_j bond at the initial condition, and the angular brackets represent the average over the 128 molecules of the same group.

The resulting self correlation functions are shown in Figure S2 with solid lines. The correlation times for the reorientations of the molecules depend not only on the groups but also the curves reveal that one bond (green lines) maintains its orientation for a time considerably longer than the other three bonds. This indicates that the molecules have preferential axes of rotation. G_{III} exhibit the strongest rotational anisotropy, followed by G_{II} and G_I and only a minor effect is observed in

Table 2: CCl_4 average reorientation frequencies w_i ($i = 1, \dots, 4$) (in ns^{-1}) for the four groups of molecules about the four possible directions of the axis of rotation. For the fastest rotational axes the inverse of the frequency w_3 is a good approximation of the average waiting time between jumps (λ^{-1}).

axis	160 K				220 K			
	G_I	G_{II}	G_{III}	G_{IV}	G_I	G_{II}	G_{III}	G_{IV}
a_1	3.91×10^{-6}	7.81×10^{-7}	1.56×10^{-6}	7.81×10^{-7}	2.80×10^{-3}	1.62×10^{-4}	3.23×10^{-4}	1.51×10^{-3}
a_2	3.83×10^{-5}	2.11×10^{-5}	7.81×10^{-7}	3.43×10^{-5}	8.30×10^{-3}	5.39×10^{-3}	9.70×10^{-4}	1.20×10^{-2}
a_3	3.62×10^{-4}	1.00×10^{-2}	1.52×10^{-3}	7.42×10^{-5}	4.76×10^{-2}	4.26×10^{-1}	9.36×10^{-2}	1.78×10^{-2}
a_4	8.59×10^{-6}	6.02×10^{-5}	7.81×10^{-7}	2.34×10^{-6}	4.36×10^{-3}	1.76×10^{-2}	8.08×10^{-4}	2.53×10^{-3}

G_{IV} . The strength of this anisotropic character decreases with increasing temperature as all the free energy barriers become relatively smaller.

During a rotation of the type $C3$ one of the C-Cl bonds remain in its place and therefore one Cl atom does not change its average position. The remaining three Cl atoms undergo a jump of 109.5 degrees. Each molecule has four possible axis for a $C3$ type rotation that coincide with the C-Cl molecular bonds. As all the molecular bonds remain lying around the four initial orientations in the crystal it is possible to define, for each molecule, four axis of rotation relative to the overall orientation of the crystal. In this way we define the axes $a_i, i = 1, \dots, 4$, for each one of the molecules in the simulation cell. The frequencies of rotational jumps for the four groups of molecules along the four possible axes of rotation, averaged over each group, are reproduced in Table 2. The numerical values of the frequencies span over four order of magnitude implying the existence of different dynamical modes in the crystal as already suggested by the rotational self correlation functions.

In order to rationalize the behavior of the functions $C_j(t)$ we developed a simple analytical model that derive these functions from the relative reorientation frequencies. We propose a master equation that describes the probabilities of occupation of the four available sites in the molecule for the Cl atoms. Let us define the stochastic variables Y_j that describe the position of the j -th Cl atom on the four available sites. Then, each Y_j takes values over a range represented by $\{1, 2, 3, 4\}$, with a probability distribution p_n^j over this range. Assuming that a reorientational jump in the molecule is a Markovian process, the master equation that describes the probability p_n^j of the state of Y_j is

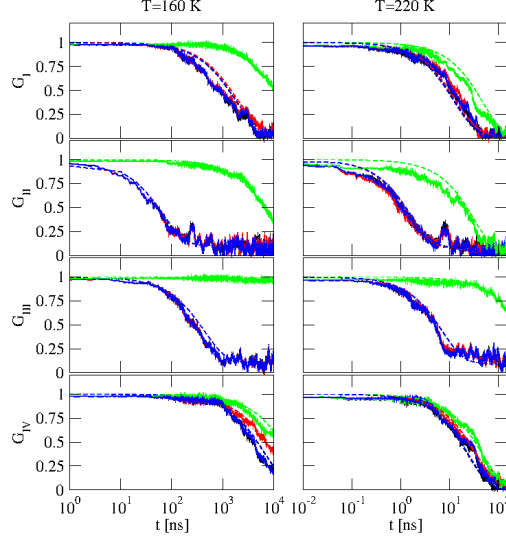


Figure S2: Auto-correlation functions $C_j(t)$ of the 4 bonds $C-Cl_j$ averaged over molecules within the four groups of the system. The solid lines correspond to the MD simulation results and the dashed lines are derived from the master equation Eq. (??). Different colors correspond to the four different bonds.

$$\frac{dp_n^j(t)}{dt} = \sum_{n'} \left[v_{nn'} p_{n'}^j(t) - v_{n'n} p_n^j(t) \right]; j = 1, \dots, 4, \quad (2)$$

where $v_{nn'}$ is the transition probability per unit time from the site n' to the site n . These equations may be written in matrix form as

$$\frac{d\vec{P}^j}{dt} = V\vec{P}^j, \quad (3)$$

where \vec{P}^j is the vector $(p_1^j(t), p_2^j(t), p_3^j(t), p_4^j(t))$, and V is the 4×4 matrix

$$\begin{pmatrix} -(v_{21} + v_{31} + v_{41}) & v_{12} & v_{13} & v_{14} \\ v_{21} & -(v_{12} + v_{32} + v_{42}) & v_{23} & v_{24} \\ v_{31} & v_{32} & -(v_{13} + v_{23} + v_{43}) & v_{34} \\ v_{41} & v_{42} & v_{43} & -(v_{14} + v_{24} + v_{34}) \end{pmatrix}. \quad (4)$$

Eq. (??) is an homogeneous first order differential equation with constant coefficients. The

solution is

$$\vec{P}^j(t) = R^{-1} e^{V_D(t)} R \vec{P}^j(0) \quad (5)$$

where R is the matrix that diagonalize V , $V_D = R V R^{-1}$. Assuming that C3 jumps are the exclusive mechanism of molecular reorientation, the $v_{nn'}$ can be approximated using the frequency of rotations w_i around the axes a_i . These frequencies were calculated from the MD simulations and are summarized in Table 2. They can be interpreted as the probabilities w_i for rotations per unit time around each one of the four possible axis. Frequencies smaller than 10^{-6} ns^{-1} correspond to less than 5 rotational jumps in $10 \mu\text{s}$ and therefore are negligible.

The tetrahedral constraint between the Cl atoms imply that a nn' transition can be achieved under two different single rotation events. Considering all rotation events as independent processes, we can calculate $v_{nn'}$ as the sum of the probability of the two possible events leading to a nn' transition. For example, $v_{12} = (w_3 + w_4)/2$, $v_{13} = (w_2 + w_4)/2$, $v_{14} = (w_2 + w_3)/2$ and so on. The factor of $1/2$ is due to the assumption that both directions of rotation are equally probably, which was tested to be statistically true.

The next step is to solve the proposed master equation with the four different initial conditions, which are $P_1^j(0) = (1, 0, 0, 0)$, $P_2^j(0) = (0, 1, 0, 0)$, $P_3^j(0) = (0, 0, 1, 0)$ and $P_4^j(0) = (0, 0, 0, 1)$. Let us denote the four corresponding solutions as $p_i^j(t)$, with $i, j = 1, \dots, 4$. Then, the rotational auto correlation functions can be expressed in terms of the solution of the master equation as

$$C_j(t) = \vec{b}_j \cdot \left[\vec{b}_1 p_1^j(t) + \vec{b}_2 p_2^j(t) + \vec{b}_3 p_3^j(t) + \vec{b}_4 p_4^j(t) \right]. \quad (6)$$

The resulting solutions $C_j(t)$ are plotted on Figure S2 using dashed lines. The agreement between the results directly measured from the simulation trajectories and those derived from the master equation is excellent, justifying the assumptions made in the derivation of the analytical model.

The statistics behind the rotational jumps can be evaluated by studying the waiting time between successive jumps around the axes a_1, \dots, a_4 . On some of the axes the rotational events are very rare and the length of our simulations do not allows to see a well defined pattern for those spe-

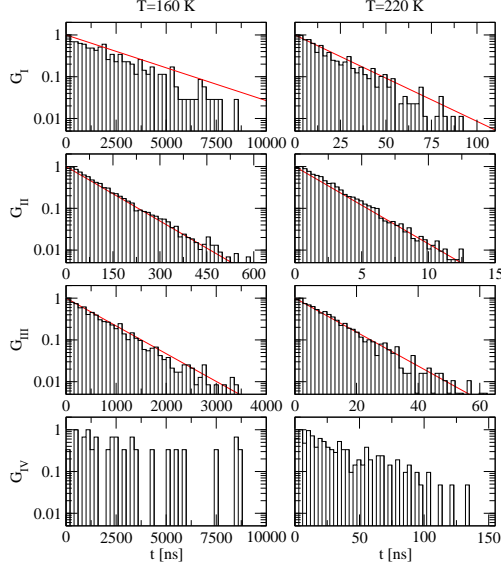


Figure S3: Distributions of waiting times for two temperatures and the corresponding Poisson curves (in red) for the fastest rotational axes of G_I , G_{II} and G_{III} .

cific slow axes. Nevertheless, for the fastest axes the process reveals itself as following a Poisson distribution. In Figure S3 we show the distribution of waiting times for rotational events around the fastest axis of rotation for each group of molecules. The histograms are directly obtained from the simulated trajectories. The solid red lines in the plots for the three fastest groups correspond to $e^{-\lambda t}$, with the Poisson parameter λ being the frequency of jumps around a_3 axes, w_3 from Table 2.

A similarity between the dynamical behavior of all the different groups could be inferred by looking at the self correlation functions $C_j(t)$ and distribution of waiting times shown in Figures S2 and S3, respectively. In particular, G_{II} and G_{III} are the two groups with the closest quantitative behavior. In order to explore whether this kinetic resemblance has a correlation with the molecular arrangement we analyzed the orientation of the fastest axis for each one of the groups. Interestingly, the fastest axes of the molecules of G_{II} and G_{III} are parallel to each other in pairs that involve the first neighbors, as shown in Figure S4. For groups G_I and G_{IV} there is a certain degree of spacial correlation, but it does not include the eight pairs of molecules of the unit cell.

NQR spectroscopy allows to measure the spin-lattice relaxation time T_1 . Since the low temperature crystalline structure of CCl_4 has four nonequivalent molecules in the unit cell, the NQR spectral lines correspond to the 16 Cl atoms of these four molecules. Then it is possible to mea-

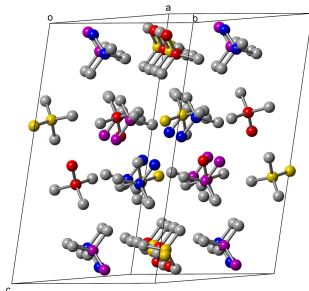


Figure S4: Unit cell displaying the molecules of groups G_I , G_{II} , G_{III} and G_{IV} in red, blue, violet and yellow respectively. The colored axis represent the fastest direction of rotation for each molecule.

sure the relaxation times T_1 , for each line, as function of temperature. As nuclear magnetization is proportional to the nuclear spin polarization, applying the slow reorientational model for T_1 by Alexander and Tzalmona³⁵ it is possible to find the reorientation relaxation time as function of the jumps probabilities ν_{nm} .

Starting from the master equation for the nuclear polarization, Zuriaga *et al*²³ proposed a model for tetrahedral molecules that allow us to find the chlorine T_1 relaxation times as a function of reorientation frequencies w_i around the four molecular axes. From the analytical model and the MD simulations, 16 relaxation times are obtained at each temperature, four for each group of molecules. The results for T_1 vs. $1000/T$ are represented in Figure S5 along with the experimental results, which also include the cases of $CBrCl_3$ and CBr_2Cl_2 .

The existence of a preferential axis of rotation for three groups (G_I , G_{II} and G_{III}) allows the identification of three short times T_{1s} of similar magnitude (corresponding to the three Cl atoms out of the fastest axis) and a long time T_{1l} (for the Cl atom on the fastest axis). The remaining group (G_{IV}) has no preferential axis of rotation and therefore the four relaxation times are all similar.

The set of 16 relaxation times from the simulations are grouped in increasing order in the following five sets:

1. The shortest time correspond to the T_{1s} describing G_{II} (green triangles).
2. The next time corresponds to T_{1s} of G_{III} (blue squares).
3. The third set is for T_{1s} of G_I (violet circles).

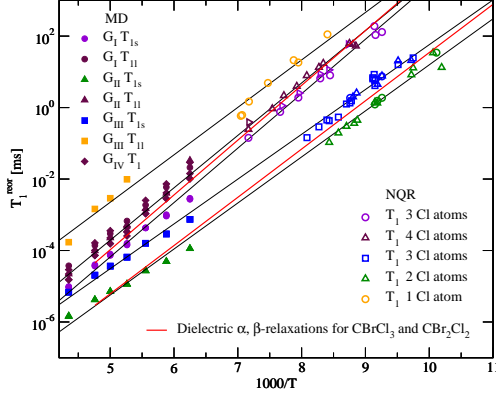


Figure S5: Spin-lattice relaxation times obtained by molecular dynamics simulations (full symbols). Results from NQR studies of CCl_4 ²³ (empty symbols) are shown. Red lines represents the behavior of τ_α (upper) and τ_β (lower) of CBrCl_3 and CBr_2Cl_2 taken from Ref.²³

4. The fourth set includes T_{II} of G_I (brown circles), T_{II} of G_{II} (brown triangles) and T_I of G_{IV} (brown diamonds).
5. The last set corresponds to T_{II} of G_{III} (orange squares).

The black straight lines in Figure S5 are the result of a linear least-squares fit of the values $\log T_1$ vs. $1000/T$, including both, simulation and experimental results.

There are three main features that arise from Figure 5. First, the simulation curves are in a good agreement with the experimental data, prolonging the same Arrhenius curves from 100 to 230 K. Second, the results for T_1 spread along two orders of magnitude in time, indicating the presence of fast and slow modes. Third, the overall behavior resembles α and β relaxation times of CBr_2Cl_2 (also shown in Figure S5) and CBrCl_3 , showing that the dynamics of the non-glass former CCl_4 has strong similarities with that of the other members of the isostructural series $\text{CBr}_n\text{Cl}_{4-n}$.

Conclusions

We performed extensive molecular dynamics simulations of CCl_4 in the monoclinic cell. By studying time reorientational auto-correlation functions as a function of temperature we found distinct behaviors for the four different C-Cl bonds in the molecule. As a consequence, different

re-orientational correlations times emerge for the four groups of nonequivalent molecules in the system: two times are enough to characterize three of the four groups and one time is associated to the remaining group.

The complete understanding of glassy systems, even in the case of the simpler rotational glasses, remains elusive in the sense that no complete theoretical picture can be drawn yet. Nevertheless, there is a general agreement on the existence of two main universal features referred to α and β relaxation. Rotational glasses of the type CBr_nCl_{4-n} , with $n=1, 2, 3$ are glass formers displaying fast and slow rotational modes as they approach to the glass transition temperature. In this paper we show that CCl_4 has essentially the same dynamical behavior, as a function of temperature, to that of its isostructural glass formers. Long molecular dynamics simulations trajectories, based on a simple pair-wise additive force-field, yield to results that are fully in line with those obtained with NQR experiments. The simulations clearly show that there are preferential axes of rotation, which are fixed with respect to the crystal orientation. Two of the inequivalent group of molecules are significantly faster than the other two, leading to a clear heterogeneity in the dynamics of the system. Moreover, it is found that the orientation of the two fast axes of rotations is the same, suggesting an overall dynamics anisotropy correlated to the molecular orientations.

Finally, our results on CCl_4 suggest that the observed heterogeneous dynamic of molecules of type $CXCl_3$ with the same crystal structure could be due to the molecular environment on the crystal and not to the breaking of the tetrahedral symmetry of the molecule. Then, it would be interesting to corroborate if there is any relation between the fastest axis in the CCl_4 molecules and the C-Br axis in the $CBrCl_3$ crystals. We are performing MD simulations to elucidate this open question.

Acknowledgement

N.B.C., M.Z. and P. S acknowledge financial support of SECYTUNC and CONICET. This work used computational resources from CCAD Universidad Nacional de Córdoba (<http://ccad.unc.edu.ar/>), in particular the Mendieta Cluster, which is part of SNCAD MinCyT, República Argentina.

Supporting Information Available

A more detailed explanation of the method for counting molecular jumps and C-C radial distribution functions at the lowest and highest simulated temperatures along with experimental C-C distances are presented as supplemental material. This material is available free of charge via the Internet at <http://pubs.acs.org/>.

References

- (1) Schneider, U.; Brand, R.; Lunkenheimer, P.; Loidl, A. Excess Wing in the Dielectric Loss of Glass Formers: A Johari-Goldstein β -Relaxation?. *Phys. Rev. Lett.*, **2000**, 84, 5560-5563.
- (2) Lunkenheimer, P.; Loidl, A. Dielectric Spectroscopy of Glass-forming Materials: α -relaxation and Excess Wing. *Chem. Phys.*, **2002**, 284, 205-219.
- (3) Affouard, F.; Cochin, E.; Danéde, F.; Decressain, R.; Descamps, M.; Haeussler, W. Onset of Slow Dynamics in Difluorotetrachloroethane Glassy Crystal. *J. Chem. Phys.*, **2005**, 123, 084501.
- (4) Ngai, K. L.; Paluch, M. Classification of Secondary Relaxation in Glass-Formers Based on Dynamic Properties. *J. Chem. Phys.*, **2004**, 120, 857-873.
- (5) Pardo, L. C.; Lunkenheimer, P.; Loidl, A. α and β Relaxation Dynamics of a Fragile Plastic Crystal. *J. Chem. Phys.*, **2006**, 124, 124911.
- (6) Johari, G. P.; Goldstein M. Viscous Liquids and the Glass Transition. II. Secondary Relaxations in Glasses of Rigid Molecules *J. Chem. Phys.*, **1970**, 53, 2372.
- (7) Ngai, K. L. Correlation Between the Secondary β -relaxation Time at T_g with the Kohlrausch Exponent of the Primary α Relaxation or the Fragility of Glass-Forming Materials. *Phys. Rev. E*, **1998**, 57, 7346-7349.

- (8) Schneider, U.; Brand, R.; Lunkenheimer, P.; Loidl, A. Excess Wing in the Dielectric Loss of Glass Formers: A Johari-Goldstein β Relaxation?. *Phys. Rev. Lett.*, **2000**, 84, 5560-5563.
- (9) Johari, G. P.; Power, G.; Vij, J. K. Localized Relaxation's Strength and its Mimicry of Glass-softening Thermodynamics. *J. Chem. Phys.*, **2002**, 116, 5908-5909.
- (10) Johari, G. P. Intrinsic Mobility of Molecular Glasses. *J. Chem. Phys.*, **1973**, 58, 1766-1770.
- (11) Capaccioli, S.; Ngai, K. L.; Shinyashiki, N. The Johari-Goldstein β -Relaxation of Water. *J. Chem. Phys. B*, **2007**, 111, 8197-8209.
- (12) Capaccioli, S.; Ngai, K. L. Resolving the Controversy on the Glass Transition Temperature of Water?. *J. Chem. Phys.*, **2011**, 135, 104504.
- (13) Jiménez-Ruiz, M.; Criado, A.; Bermejo, F.J.; Cuello, G.J.; Trouw, F.R.; Fernández-Perea, R.; Löwen, H.; Cabrillo, C.; Fischer, H. E. Purely Dynamical Signature of the Orientational Glass Transition. *Phys. Rev. Lett.*, **1999**, 83, 2757-2760.
- (14) Jiménez-Ruiz, M.; González, M. A.; Bermejo, F.J.; Miller, M. A.; Birge, N. O.; Cendoya, I.; Alegría, A. Relaxational Dynamics in the Glassy, Supercooled Liquid, and Orientationally Disordered Crystal Phases of a Polymorphic Molecular Material. *Phys. Rev. B*, **1999**, 59, 9155-9166.
- (15) Voguel, M.; Rossler, E. On the Nature of Slow β -Process in Simple Glass Formers: A ^2H NMR Study. *J. Phys. Chem. B*, **2000**, 104, 4285-4287.
- (16) Voguel, M.; Rossler, E. Slow β Process in Simple Organic Glass Formers Studied by one- and two-dimensional ^2H Nuclear Magnetic Resonance. I. *J. Chem. Phys.*, **2001**, 114, 5802.
- (17) Romanini, M.; Negrier, Ph.; Tamarit, J. Ll.; Capaccioli, S.; Barrio, M.; Pardo, L. C.; Mondieig, D. Emergence of Glassy-like Dynamics in an Orientationally Ordered Phase. *Phys. Rev. B*, **2012**, 85, 134201.

- (18) Drozd-Rzoska, A.; Rzoska, S.J.; Pawlus, S.; Tamarit, J. L. Dynamics Crossover and Dynamic Scaling Description in Vitrification of Orientationally Disordered Crystal. *Phys. Rev. B*, **2006**, 73, 224205.
- (19) Martinez-Garcia, J.C.; Tamarit, J. L.; Rzoska, S. J. Prevalence for the Universal Distribution of Relaxation Times Near the Glass Transitions in Experimental Model systems: Rodlike Liquid Crystals and Orientationally Disordered Crystals. *J. Chem. Phys.*, **2011**, 134, 144505.
- (20) Martinez-Garcia, J.C.; Tamarit, J. L.; Rzoska, S. J. Enthalpy Space Analysis of the Evolution of the Primary Relaxation Time in Ultraslowing Systems. *J. Chem. Phys.*, **2011**, 134, 024512.
- (21) Martinez-Garcia, J.C.; Tamarit, J. L.; Capaccioli, S.; Barrio, M.; Veglio, N.; Pardo, L. C. α -relaxation Dynamics of Orientationally Disordered Mixed Crystals Composed of Cl-adamantane and CN-adamantane. *J. Chem. Phys.*, **2010**, 132, 164516.
- (22) Caballero, N. B.; Zuriaga, M.; Carignano, M.; Serra, P. The Plastic and Liquid Phases of CCl_3Br Studied by Molecular Dynamics Simulations. *J. Chem. Phys.*, **2012**, 136, 094515.
- (23) Zuriaga, M. J.; Perez, S. C.; Pardo, L. C.; Tamarit, J. Ll. Dynamic Heterogeneity in the Glass-Like Monoclinic Phases of $\text{CBr}_n\text{Cl}_{4-n}$, $n = 0,1,2$. *J. Chem. Phys.*, **2012**, 137, 054506.
- (24) Zuriaga, M.; Pardo, L.C.; Lunkenheimer, P.; Tamarit, J. Ll.; Veglio, N.; Barrio, M.; Bermejo, F.J.; Loidl, A. New Microscopic Mechanism for Secondary Relaxation in Glasses. *Phys. Rev. Lett.*, **2009**, 103, 075701.
- (25) Pardo, L. C.; Barrio, M.; Tamarit, J. L.; López, D. O.; Salud, J.; Negrier, P.; Mondieig, D. Miscibility Study in Stable and Metastable Orientational Disordered Phases in a Two-Component System $(\text{CH}_3)\text{CCl}_3 + \text{CCl}_4$. *Chem. Phys. Lett.*, **1999**, 308, 204-210.
- (26) Pardo, L. C.; Barrio, M.; Tamarit, J. L.; López, D. O.; Salud, J.; Negrier, P.; Mondieig, D. First Experimental Demonstration of Crossed Isodimorphism: $(\text{CH}_3)_3\text{CCl} + \text{CCl}_4$ Melting Phase Diagram. *Phys. Chem. Chem. Phys.*, **2001**, 3, 2644-2649.

- (27) Pardo, L. C.; Barrio, M.; Tamarit, J. L.; Negrier, P.; López, D. O.; Salud, J.; Mondieig, D. Stable and Metastable Phase Diagram of the Two-Component System $(\text{CH}_3)_3\text{CCl}-(\text{CH}_3)\text{CCl}_3$: An Example of Crossed Isodimorphism. *J. Phys. Chem. B*, **2001**, 105, 10326-10334.
- (28) Pardo, L. C.; Barrio, M.; Tamarit, J. L.; López, D. O.; Salud, J.; Negrier, P.; Mondieig, D. Stable and Metastable Orientationally Disordered Mixed Crystals of the Two-Component System $(\text{CH}_3)_2\text{CCl}_2+\text{CCl}_4$. *Chem. Phys. Lett.*, **2000**, 321, 438-444.
- (29) Pothoczki, Sz.; Ottochian, A.; Rovira-Esteva, M.; Pardo, L. C.; Tamarit, J. Ll.; Cuello, G. J. Role of Steric and Electrostatic Effects in the Short-Range Order of Quasitetrahedral Molecular Liquids. *Phys. Rev. B.*, **2012**, 85, 014202.
- (30) Ohta, T.; Yamamuro, O.; Matsuo, T. Heat Capacities and Phase Transitions of CBrCl_3 and CBr_2Cl_2 . *J. Phys. Chem.*, **1995**, 99, 2403-2407.
- (31) Binbrek, O. S.; Lee-Dadswell, S. E.; Torrie, B. H.; Powell, B. M. Crystal Structures of Dibromodichloromethane and Bromotrichloromethane. *Mol. Phys.*, **1999**, 96, 785-794.
- (32) Zuriaga, M.; Carignano, M.; Serra, P. Rotational Relaxation Characteristics of the Monoclinic Phase of CCl_4 . *J. Chem. Phys.*, **2011**, 135, 044504.
- (33) Cohen, S.; Powers, R.; Rudman, R. Polymorphism of the Crystalline Methylchloromethane Compounds. VI. The Crystal and Molecular Structure of Ordered Carbon Tetrachloride. *Acta Cryst. B*, **1979**, 35, 1670-1674.
- (34) Carter, N. J.; Cross A. Mechanics of the Kinesin Step. *Nature*, **2005**, 435, 308.
- (35) Alexander, S.; Tzalmona, A. Measurement of Molecular Rotation by N^{14} Nuclear Quadrupole Resonance Relaxation Times. *Phys. Rev. Lett.*, **1964**, 13, 546-547.

Dynamic Heterogeneity In The Monoclinic Phase Of CCl₄

Supporting Information

Method for Detecting Rotational Jumps

In order to detect the rotational jumps of the CCl₄ molecules we perform a detailed analysis of the trajectories based on an algorithm published by N. J. Carter and A. Cross; *Nature* **435** 308 (2005). Let us consider the coordinates of each one of the Cl atoms, relative to their bonded C atom, and denote them by $r_{n,\alpha,i}$. Here α represent any of the Cartesian coordinates x , y or z ; the index n denote molecule and $i = 1, 2, 3, 4$ refers to each one of the Cl atoms of molecule n .

$$f_{n,\alpha,i}(t) = \frac{\langle r_{n,\alpha,i} \rangle_- - \langle r_{n,\alpha,i} \rangle_+}{\sqrt{\frac{S_-}{\Delta t} + \frac{S_+}{\Delta t}}} \quad (7)$$

where the angular brackets represent time average, the subindices $-$ and $+$ indicate the lapse of length Δt before and after time t , respectively; and S_- and S_+ are the corresponding standard deviations. Whenever there is a rotational jump the mean values and standard deviation are affected. Consequently, the test function $f_{n,\alpha,i}(t)$ reflects those changes with a spike. The spike could be upwards or downwards depending on the direction of change of the average coordinate.

In order to have a single function per molecule, the twelve individual $f_i(t)$ for an individual molecule can be combined in the following way:

$$\mathcal{F}_n(t) = \sum_{i=1,2,3,4} \sum_{\alpha=x,y,z} |f_{n,\alpha,i}(t)| \quad (8)$$

By careful inspection of the simulation trajectories and the response of the test functions we selected a time lapse $\Delta t = 50$ ps. In Figure S6 we show an example of the variation of the relative coordinates $x_{n,\alpha,i}(t)$ corresponding to the four Cl atoms of molecule n , which undergoes a jump

at $t = 2971.39$ ns. The figure also shows the corresponding four individual response functions of each Cl atom:

$$F_{n,i}(t) = \sum_{\alpha=x,y,z} |f_{n,\alpha,i}(t)| \quad (9)$$

along with the final curve of the test function $\mathcal{F}_n(t)$. A threshold value of $\mathcal{F}_n(t)=50$ was used to determine the rotational jumps.

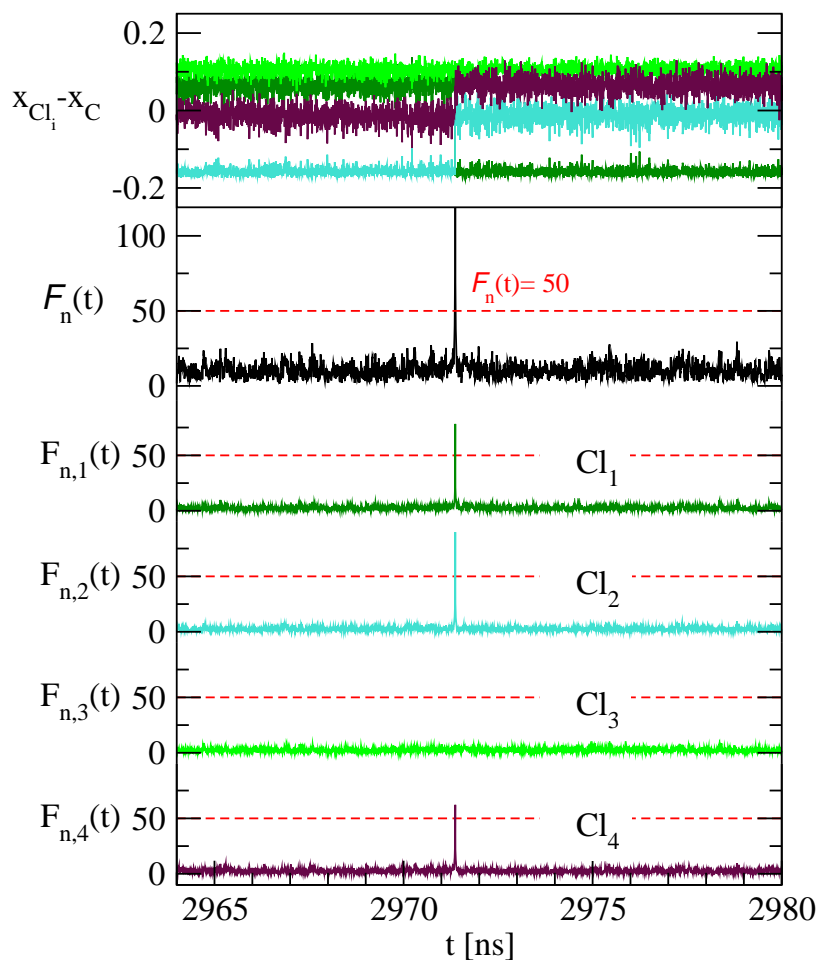


Figure S6: Top: Variation of the relative x coordinates of the four Chlorine atoms of molecule n in green (Cl₁), cyan (Cl₂), light green (Cl₃) and orange (Cl₄). The four individual response functions are also shown in the corresponding color, along with the final curve of the test function (in black). The threshold value of 50 is shown in red.

Radial Distribution Functions

In order to analyze the crystalline structure of the simulation supercell, we calculated the Carbon-Carbon radial distribution function for each possible combination of Carbon atoms within the different 4 groups of molecules in the system, at the all the simulation temperatures. We observed a good agreement of the function's peaks with the experimental values for the Carbon-Carbon distances on the monoclinic cell. On figure *S7* we show the results at the lowest and highest simulation temperatures.

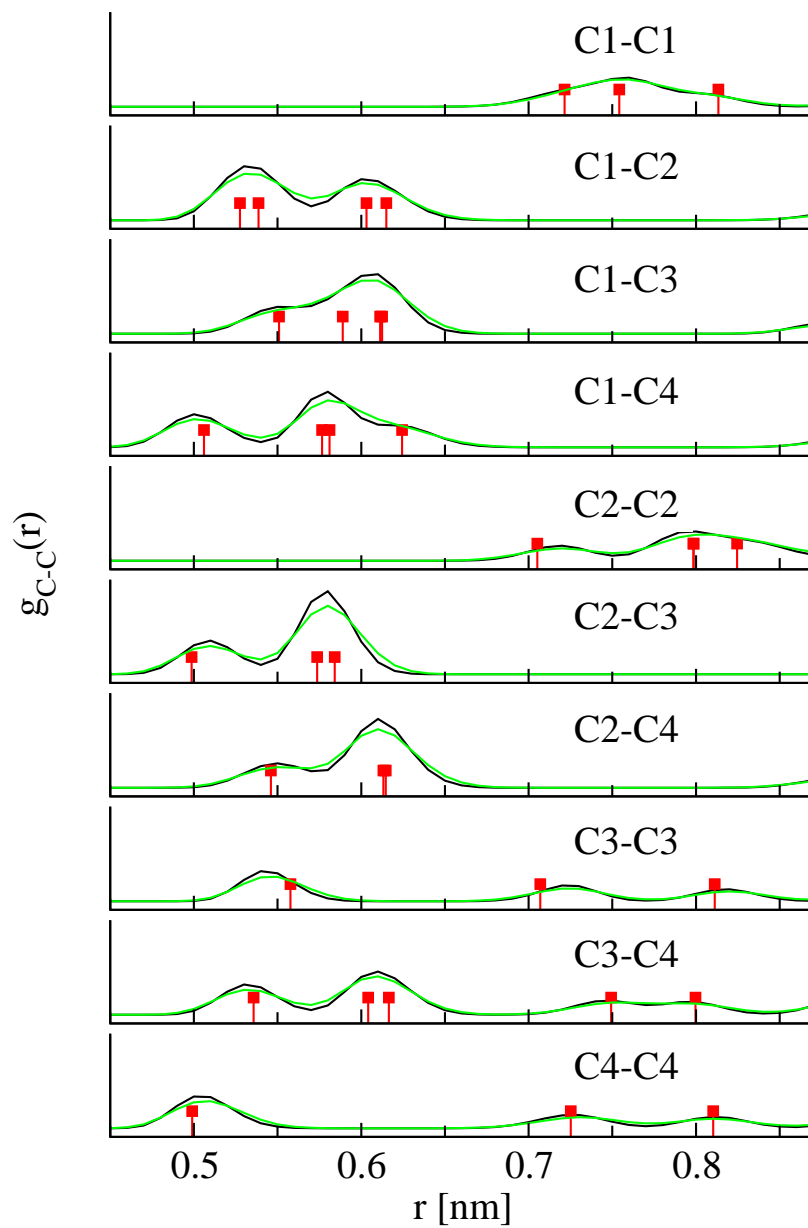


Figure S7: Carbon-Carbon radial distribution function for all possible combination of groups in the system at 160 K (black line) and 220 K (green line). On the graph the experimental values are also shown in red.